Effect of the Loading of Di- and Tri-valent Metal Cations on the Performance of Sulfated Silica-titania Nano-catalyst in the Esterification Reaction

Khalid Al-Qaysi [1], Hamed Nayebzadeh [2]*, Naser Saghatoleslami [3], and Jabbar Gardy [4]

[1] Department of Chemical Engineering, University of Technology, Baghdad, Iraq

[2] Faculty of Material and Chemical Engineering, Esfarayen University of Technology, Esfarayen, North Khorasan, Iran

[3] Department of Chemical Engineering, Faculty of Engineering, Ferdowsi University of Mashhad, Mashhad, Iran

[4] School of Chemical and Process Engineering, Faculty of Engineering and Physical Sciences, University of Leeds, West Yorkshire, Leeds, LS2 9JT, United Kingdom

ARTICLE INFO

ABSTRACT

In this study, a series of sulfated silica-titania catalysts were modified by metal cations (Al, Co, Zr, Cr, and Zn) to enhance the catalytic activity and stability of sulfated silica-titania in the esterification reaction. The results indicated that the sulfate phases of sulfated silica-titania were mostly changed to $TiO(SO_4)$ by the incorporation of support cations. It affected the acidity content of the samples and the bonding strength between the sulfate group and the support surface. Moreover, the mean pore size was drastically increased which had a positive influence on the activity of the sample in the esterification reaction. The results of catalytic activity showed that all the samples had suitable activity at 120°C, whereas the sulfated silica-titania catalyst that was reinforced by Al^{3+} exhibited less activity reduction by setting the temperature to 90°C. The highest conversion of oleic acid (90.7 ± 2%) was obtained under optimal reaction conditions including the temperature of 90°C, methanol/oleic acid molar ratio of 9:1, 3 wt.% catalyst, and reaction time of 3 h. The sulfated silica-titania modified by Al^{3+} also exhibited good catalytic stability for six cycles while a high reduction in the activity of sulfated silica-titania catalyst was observed.

INTRODUCTION

Due to the ever-increasing energy demand and the problems associated with consuming petroleum fuels, there is a strong driving force worldwide to develop alternative fuels in order to reduce greenhouse gases [1]. Most petroleum fuels are consumed in the transportation system.

Therefore, it is necessary to use a renewable fuel that can be utilized in the current engines. Among alternative fuels, biodiesel, which is usually made via the esterification/transesterification process from animal fat/vegetable oils and methanol in the presence of a catalyst [2], presents suitable properties for replacing the petroleum fuel due

* *Corresponding Author Email: h.nayebzadeh@esfarayen.ac.ir*

to its low toxicity, biodegradability, low emissions, and compatibility with current diesel engines. Therefore, the production of biodiesel fuels has increased over the last 20 years [3].

The industrial process of biodiesel production, which is usually performed on raw vegetable oils and homogeneous alkaline catalyst, is faced with major challenges and has to be modified due to the increase of deforestation for oil seed cultivation, conflict of demand between human nutrition and fuel production as a result of using vegetable oils, and the long and costly downstream process (separations, purification, and neutralization) which increases the biodiesel cost [4]. In this regard, utilizing the used and nonedible feedstock (waste cooking oil, Jatropha oil, etc.) and microalgae oil has been proposed in the second and third generations of biodiesel production. Although the production cost decreases considerably by reducing the feedstock price, the downstream cost increases significantly due to the reaction between the homogenous alkaline catalyst (NaOH or KOH) and free fatty acids (FFAs) of the feedstock (usually nonedible oil has FFA > 1 wt.%).

In order to overcome such demerits, many researchers have studied heterogeneous catalysts for simultaneous esterification and transesterification processes of cheap feedstocks for biodiesel production [5]. According to the literature, most heterogeneous catalysts consist of two parts which are the catalyst support and the active phase. Catalyst supports have to be thermally stable and have a high surface area. This structure allows FFAs and triglyceride molecules access to the active sites of the catalyst and the internal surface area [6]. Various metal oxides , including silica [7], titania [8], alumina [9], and zirconia [10, 11] have been significantly highlighted as catalyst supports over recent years. Silica and titania are widely studied due to their favorable properties, including high surface area, low cost, porous structure, acidity, good mechanical and chemical stability, low toxicity, and easy availability [12, 13].

In order to achieve higher activity and stability as well as minimum structural weakness, bifunctional catalyst supports have been widely studied. Mahmoud et al. [14] synthesized ZrO_2/SiO_2 catalysts for stearic acid esterification and reported that the most active catalyst (ZrSiOC) exhibited good reusability until five runs. SiO_2-Al_2O_3

supported bifunctional acid-base presented high activity and reusability [15, 16]. Kulyk et al. [17] reported that TiO_2-SiO_2 and Al_2O_3-SiO_2 are proper catalysts. The ZnO-SiO_2 nanocomposite has been used for biodiesel production and has obtained over 95% yield [18, 19]. Cobalt, chromium, calcium, etc. have been tested to obtain high active and stable catalyst support [20-22].

The active phase is usually chosen from acid or base components and is modified on the support with the impregnation method [23, 24]. Sulfated metal oxide is a good example of a solid super-acid catalyst and shows more tolerance to high amounts of FFAs, moisture, and other impurities [25, 26]. Manga et al. [27] investigated the activity of SO_4^{2-}/TiO_2-SiO_2 catalysts and a 98.89% ethyl ester conversion was achieved with 5 wt.% catalyst, a molar ratio of 13, and a reaction time of 2.25 h. Shao et al. [28] fabricated a sulfated silica-titania catalyst via the sol-gel method followed by calcination at different temperatures. It was reported that the sulfated silica-titania catalyst exhibited less stability after the first run and the conversion also reduced by 60%. A similar conclusion was drawn by Sheikh et al. [29] for the esterification of oleic acid over sulfated silica-titania (50% reduction in the conversion after the first run).

The instability of sulfated titania, silica, and titania-silica catalysts in the esterification and transesterification reactions are mainly related to the leaching of sulfate groups (weak bonds between the sulfate groups and the surface of the catalyst support) [28, 30]. Application of metal cations that make strong bonds with the sulfate group can overcome this weakness. As a result, the preparation of tri-functional catalysts has been suggested. Li et al. [31] modified SO_4/TiO_2-SiO_2 with La^{3+} ions and found that the stability improved significantly, owing to the strong bonding of Si and La^{3+} ions with the sulfate groups. The La^{3+}/ZnO-TiO_2 tri-functional catalyst was utilized for biodiesel production from waste cooking oil by esterification of FFAs and showed high activity (over 96%) and stability (used for five cycles). Feyzi and Shahbazi [32] synthesized Cs–Ca/SiO_2–TiO_2 nanocatalysts for biodiesel production which obtained higher activity and stability compared with SiO_2–TiO_2 nanocatalysts. Based on previous research on bifunctional nanocatalysts including evaluations of the interaction between SiO_2 or TiO_2 and zirconia [33, 34], iron oxide [35], alumina

[36, 37], and zinc oxide [38, 39], these cations can be suitable options to improve the weakness of sulfated silica-titania nanocatalysts.

To the best of the authors' knowledge, there is a lack of studies on the modification of sulfated silica-titania catalysts in order to synthesize a tri-functional nanocatalyst with a proper catalytic activity and stability in the esterification reaction. Therefore, herein we report the preparation of a sulfated silica-titania catalyst modified by various metal cations with different valances (Zn^{2+}, Co^{2+}, Al^{3+}, Cr^{3+}, and Zr^{4+}). The solid acid catalysts synthesized via a combined sol-gel and impregnation method were characterized using X-ray diffraction (XRD), Fourier-transform infrared spectroscopy (FTIR), Brunauer-Emmett-Teller (BET) surface area, field emission scanning electron microscopy (FESEM), and titrimetric analyses (the Hammett indicator method). The catalytic activity and stability of the synthesized catalysts were also examined in the esterification of oleic acid. Finally, the parameters of the esterification reaction were optimized.

MATERIALS AND METHODS
Synthesis of catalysts

Mixed metal oxide catalysts containing titania and silica as the main components were synthesized via the sol-gel method [40, 41] as follows:

Titanium dioxide (98% purity, Merck Co.) was dispersed in a beaker containing the desired amount of nitric acid solution (4 M, Sigma-Aldrich). Then, tetraethyl orthosilicate (TEOS, 98% purity, ACROS Organics) with a constant Si/Ti molar ratio of 0.8 was added to the mixture. In order to enhance the activity of the Si-Ti complex metal oxide, other nitrate salts of metal cations, including $Al(NO_3)_3.9H_2O$ (Merck Co.), $Co(NO_3)_2.6H_2O$ (Merck Co.), $ZrO(NO_3)_2.xH_2O$ (Sigma-Aldrich), $Cr(NO_3)_3.9H_2O$ (Merck Co.), and $Zn(NO_3)_2.6H_2O$ (Merck Co.), at a metal cation/Ti molar ratio of 0.2 were separately added.

In order to form the metal cation complex, citric acid as a complex agent with a ratio of 1.5 times of metal cations was added to the previous solutions and the mixtures were continuously stirred under reflux at 80°C. The resulting mixtures were then heated to evaporate the water and the obtained viscous gels were aged overnight. Finally, the gels were dried in an oven at 110°C and calcined in air at 550°C for 4 h. The same procedure was repeated

for fabricating a silica-titania support without the addition of other nitrate salts.

The supports were activated by the modification of the sulfate group. In this regard, the sulfate groups were impregnated on the synthesized catalyst supports to enhance the catalytic activity towards the esterification reaction. For this purpose, 12.5 mL of H_2SO_4 solution (1 M, Shimi-Pjouhesh, 96%) was mixed with 1 g of the catalyst support and refluxed at 80°C for 2 h [42]. The mixtures were then oven-dried overnight at 110°C, prior to calcination under air at 550°C for 4 h. The $SO_4/SiO_2–TiO_2$ promoted by Al^{3+}, Co^{2+}, Zr^{4+}, Cr^{3+}, and Zn^{2+} were labeled as S/Al-SiTi, S/Co-SiTi, S/Zr-SiTi, S/Cr-SiTi, and S/Zn-SiTi, respectively.

Catalyst characterization

Powder X-ray diffraction (XRD, UNISANTIS XMD 300) was utilized to determine the crystal structure of the synthesized catalysts. The test was performed using Cu K_α radiation and scanned in the range of 10-80° (2θ) at rating of 10°/min. The surface functional groups of catalysts were analyzed by FT-IR spectroscopy in the range of 4000-400 cm^{-1} using a Thermo Nicolet AVATAR 370 spectrometer. The textural properties of the synthesized catalysts were determined by multipoint nitrogen adsorption-desorption method at -196 °C using AUTOSORB 1 analyzer (Quantachrome Co.). All samples were degassed at 120 °C for 8 h. Particle shape, morphology and elemental composition of the synthesized catalysts were detected using a field emission scanning electron microscope (FESEM, TESCAN Mira 3-XMU, Czech Republic) coupled with energy dispersive X-ray spectrometer (EDS). The acid strength and amount of acid sites on the surface of the synthesized catalysts were measured by Hammett indicator method in which methyl red (Hammett acidity function H_0 ≤+4.8), p-dimethylaminoazobenzene (H_0 ≤ +3.3), crystal violet (H_0 ≤+0.8) and dicinnamalacetone (H_0 ≤ -3.0) were used as indicators. The acidity was determined using titration the discolored solution by 0.01 N n-butylamine solution [11].

Esterification reaction

Esterification reaction was performed in an autoclave stainless steel reactor equipped with a thermocouple (Type-K) and a manometer. 20 g of oleic acid (Fluka Analytical, ≥99.0%), 0.6 g of catalyst and 25.8 mL methanol were added to the reactor at room temperature [11]. The mixture

was then stirred and heated at 90 °C and 120 °C for 4 h. Afterward, the ester (methyl oleate) layer was separated from the catalyst and by-product (water) by centrifugation at 4000 rpm for 20 min. The obtained methyl oleate was slowly heated to remove excess methanol and water and then titrated with 0.1 M alcoholic potassium hydroxide solution to obtain the acid value. The conversion was calculated according to the follow equations (Eqns. 1 & 2) [38]:

$$Conversion = \frac{AV_{Oleic\ acid} - AV_{Methyl\ oleate}}{AV_{Oleic\ acid}} \times 100 \quad (1)$$

$$AV = \frac{5.611\ V}{W} \quad (2)$$
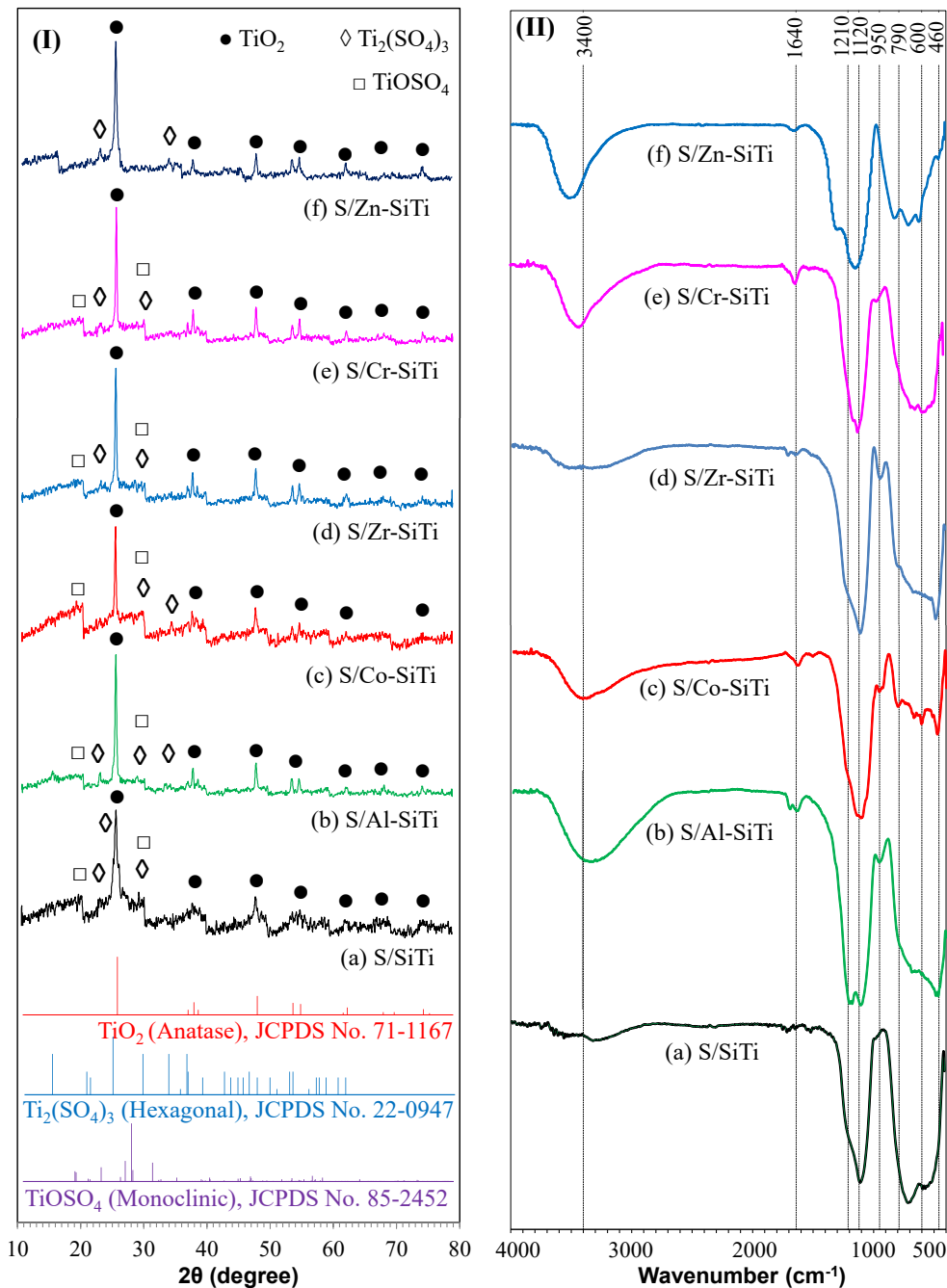
Fig. 1. (I) XRD and (II) FTIR plots of sulfated (a) silica-titania catalyst, and those silica-titania catalysts modified by (b) aluminum, (c) cobalt, (d) zirconium, (e) chromium and (f) zinc cations

where AV is the acid value, V is the volume of 0.1 M alcoholic solution of KOH used for titration, and W is the sample weight.

RESULTS AND DISCUSSION
Characterization of the synthesized solid acid catalysts
XRD analysis

The XRD patterns of the synthesized catalysts are shown in Fig. 1(I). As can be seen, the diffraction peaks of the SO_4/SiO_2–TiO_2 catalyst confirm the anatase phase of titania (JCPDS No. 71-1164) linked with the sulfate groups to form titanium oxysulfate ($TiO(SO_4)$, JCPDS No. 85-2452) and $Ti_2(SO_4)_3$ (JCPDS No. 22-0947). No characteristic peak was observed for the SiO_2 particles, which may suggest that SiO_2 diffused in the titania lattice to form a Ti–O–Si structure or an amorphous structure that would be found in the FTIR analysis [28, 43]. The SO_4/SiO_2–TiO_2 catalyst supported by metal cations (Al, Co, Zr, Cr, and Zn) leads to the formation of narrower peaks with higher intensity (and probably higher crystallinity degree; e.g. 2θ observed at 25.3°).

The results also revealed that no characteristic peaks related to the crystalline reinforced metal cations were observed, which indicated that the metal cations were probably doped into the titania lattice [44]. The overall diffraction peaks may confirm the homogenous distribution of the reinforcing metal cations within the structure of the silica-titania catalyst support [45].

The loading of sulfate groups on the support

also changed the chemical and crystal structure of titania into $TiO(SO_4)$, and the $Ti_2(SO_4)_3$ phase mostly disappeared in the case of modification with the Al^{3+} cation. It was reported that $TiO(SO_4)$ was much more active than $Ti_2(SO_4)_3$ and could transform into other sulfate phases at high concentrations of sulfate groups [46]. Based on this result, the loading of metal cations on the catalyst supports predominated the formation of the $TiO(SO_4)$ phase by replacing one oxygen atom from the titania crystals.

The summary of the calculation of the crystallite size based on the strongest peak (2θ at 25.3°) of the catalysts using Scherer's equation [47] is presented in Table 1. The results revealed that the crystallite size was significantly reduced due to the diffusion of the metal cations into titania lattice and the change of crystal sheet bonds [48]. The difference in the crystallite size can be due to the difference of the atomic radius and the valence electron of metal cations.

FTIR analysis

The FTIR spectra of the synthesized catalysts are presented in Fig. 1(II). The broad band at 3400 cm^{-1} and the weak band at 1640 cm^{-1} are related to the O-H stretching and bending vibrations, respectively [49]. The band in the region of 1000-1500 cm^{-1} can be attributed to the vibration of S=O symmetric and asymmetric vibrations [33, 50].

The strong band at 960 cm^{-1} is attributed to the Ti–O–Si vibrations in the nano-structured frameworks [51]. Moreover, the peak for M=O–S

Table 1. Physico-chemical properties of sulfated silica-titania catalyst and those sulfated silica-titania catalysts modified by various metal cations

Catalyst label code	Crystalline size (nm)[a]	Texture properties [b]			Acid properties [c]	
		S_{BET} (m²/g)	D_p (nm)	V_p (cm³/g)	Acid strength	Total acidity (mmol/g)
S/SiTi	27.1	220±1	6.6±0.1	0.55	-3.0<H_0<-8.2	1.39
S/Al-SiTi	20.7	184±1	8.9±0.1	0.63	-3.0<H_0<-8.2	1.98
S/Co-SiTi	23.5	158±1	9.1±0.1	0.55	-3.0<H_0<-8.2	1.27
S/Zr-SiTi	21.4	138±1	8.4±0.1	0.43	-3.0<H_0<-8.2	1.07
S/Cr-SiTi	24.3	206±1	7.8±0.1	0.61	-3.0<H_0<-8.2	1.05
S/Zn-SiTi	18.9	146±1	6.8±0.1	0.46	-3.0<H_0<-8.2	1.04

[a] Measured by Scherer's equation based on the peak at 25.3°
[b] calculated by BET method (S_{BET}: surface area; D_p: mean pore diameter; V_p: pore volume)
[c] Hammett indicator method

(M=metal cation) can also be detected in this region and overlaps with the vibrational peak for Ti–O–Si. The band is more visible for the silica-titania catalyst modified by Al, Co, and Zr cations. A strong interaction between the sulfate groups and metal cations leads to an increase in the stability of the catalyst [37]. Moreover, the formation of the tetrahedral framework through the Si–O–Ti bond increases the acid sites in the catalyst which can enhance the activity of the catalyst in the esterification reaction [52]. The broad peaks that appeared in the range of 550-900 cm^{-1} are attributed to the M–O–M bridging stretches such as Ti–O–Ti and Si–O–Si for the S/SiTi catalyst [53].

BET-BJH analysis

In general, a larger surface area and a bigger pore size in the catalysts facilitate the accessibility of the reactant molecules (triglyceride/FFA) to the external and internal acid sites. As can be seen from Table 1, the loading of metal cations (Al, Co, Zr, Cr, and Zn) on the sulfated silica-titania catalyst resulted in a relatively lower surface area compared with the sulfated silica-titania catalyst. This is probably due to the particle surface coverage by the modified metal cations [36]. However, an insignificant change was observed in the mean pore diameter and pore volume.

The N_2 adsorption-desorption curves and insets of the pore size distribution for the sulfated silica-titania and sulfated silica-titania catalyst modified with various metal cations are illustrated in Fig. 2. It can be seen that the adsorption-desorption isotherm for all the synthesized catalysts is type IV
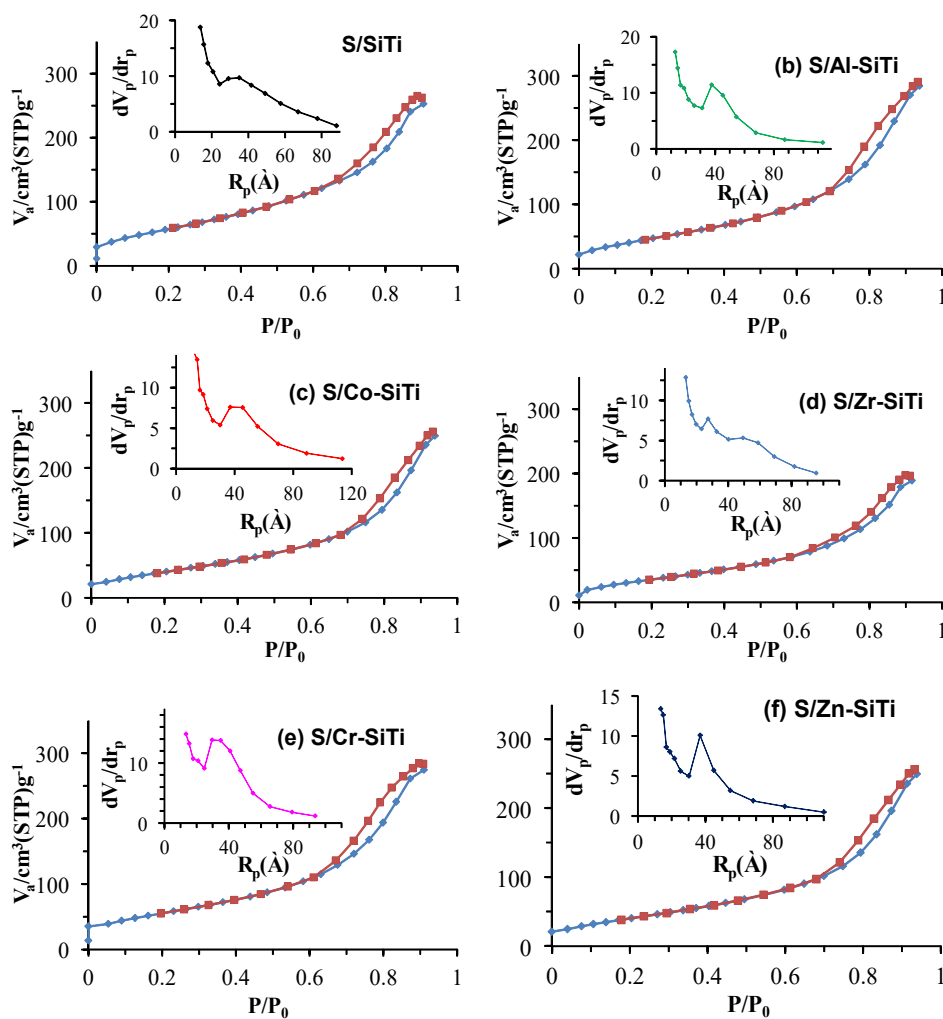
Fig. 2. N_2 Adsorption-desorption hysteresis and the pore size distribution (insets) for (a) sulfated silica-titania catalyst and those sulfated silica-titania catalyst modified by (b) aluminum, (c) cobalt, (d) zirconium, (e) chromium and (f) zinc cations

corresponding to the mesoporous materials [54]. Moreover, the hysteresis loop of the samples is assigned to type H1, which is witnessed for the cylindrical and spherical pores [3, 55].

Acidity analysis

The catalytic activity of a catalyst has a direct relationship with its acid sites (see Table 1). According to the Hammett indicator measurement, all the synthesized catalysts present an acid strength between 48%–90% sulfuric acid (-3.0 < H_0 < -8.2). The number of acid sites on a solid surface, which was measured by amine titration, indicated that the sulfated silica-titania catalyst reinforced by alumina had the highest acidity. This was also consistent with the FTIR results in which the S/Al-SiTi catalyst exhibited sulfate bands with higher intensity.

FESEM analysis

The FESEM images of S/SiTi and S/Al-SiTi catalysts are illustrated in Fig. 3. The sulfated silica-titania catalyst showed agglomerated clusters with large particles. In the case of the catalyst support modified by Al^{3+} cations, however, a smaller particle size with lower agglomeration and more obvious external pores was observed. This morphology leads to the dispersion of sulfate groups on the surface of individual particles and inside the pores to make stronger bonds with the support surfaces (Al-SiTi).

The surface particle size of S/SiTi and S/Al-SiTi nanocatalysts was measured and the distribution histograms are depicted in Fig. 4. The size of surface particles was reduced by the loading of Al^{3+} ions such that S/SiTi had a particle size in the range of 5-25 nm and the particle size of S/
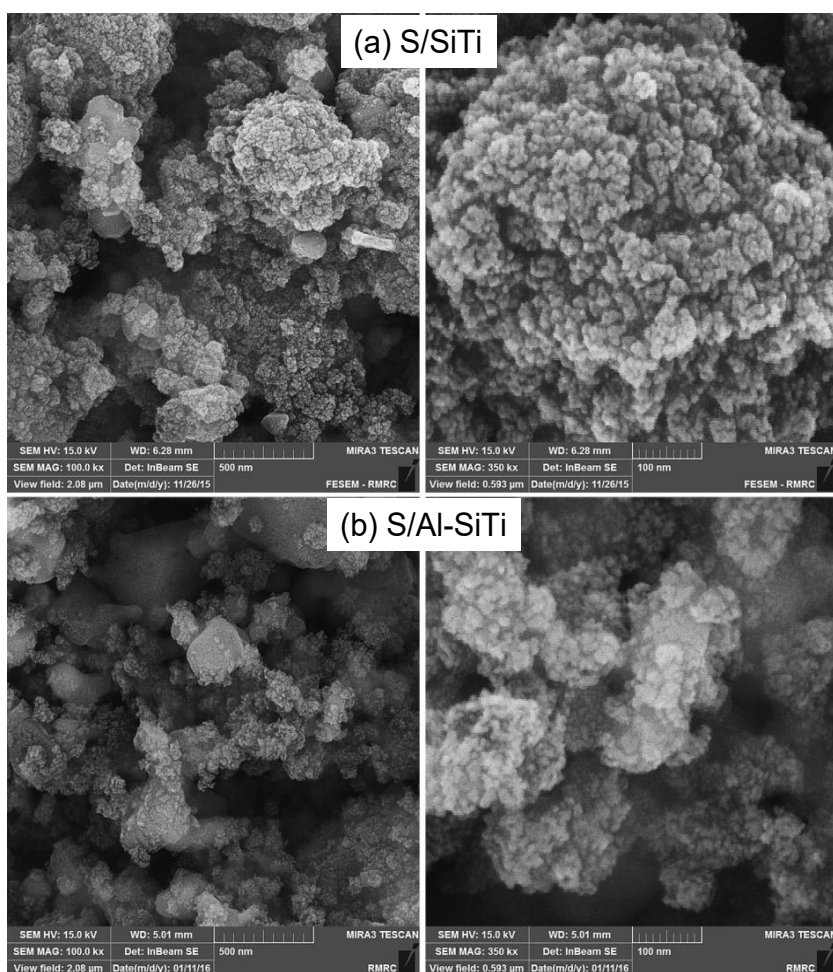
Fig. 3. FE-SEM images of (a) sulfated silica-titania catalyst and (b) sulfated silica-titania catalyst modified by aluminum cation
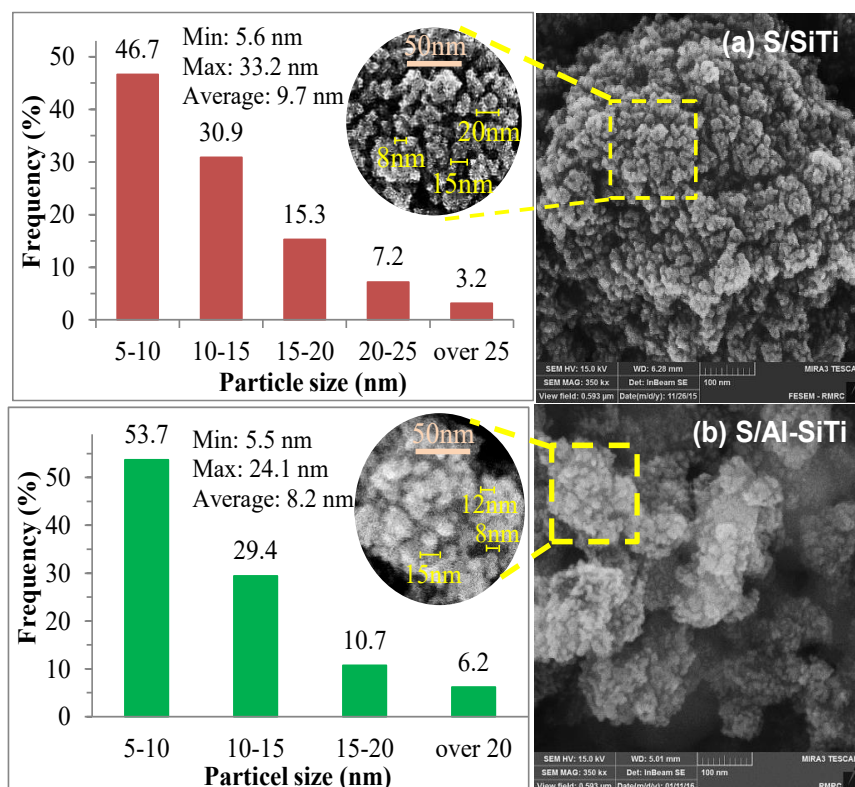
Fig. 4. Surface particle size distribution histogram of (a) sulfated silica-titania catalyst and (b) sulfated silica-titania catalyst modified by aluminum cation

Al-SiTi was lower than 25 nm. These findings were in good agreement with the crystallite size of catalysts listed in Table 1. Moreover, the frequency of particles with a size below 10 nm increased by the doping of Al^{3+} ions. In addition, the average particle size reduced from 9.7 nm to 8.2 nm by incorporating Al^{3+} ions into the SiO_2-TiO_2 structure. Reduction of particle size can enhance the interaction of sulfated groups with the surface support and consequently, increase the catalytic activity of the Al-promoted catalyst.

The surface roughness of the samples was also evaluated by analyzing the FESEM images as illustrated in Fig. 5. The 3D surface overview reveals that the surface roughness was also reduced by the doping of Al^{3+} ions. Reduction of the surface roughness by incorporating the Al^{3+} cation had a positive influence on the interaction of the reactants and active phases on the surface of the catalyst [56]. Better interaction between the reactants and the surface of the catalyst leads to the formation of higher amounts of the product. Moreover, simple egression of the product from the catalyst surface with lower roughness was

reported [57]. Therefore, it seems that S/Al-SiTi can have better interaction with the reactants in order to produce ester (biodiesel).

EDS analysis

The EDS analysis of S/SiTi and S/Al-SiTi catalysts is shown in Fig. 6. The samples only showed the cations used in the parent solution (the mixture of precursors) and no other impurities were detected. The EDS analysis confirmed the better bonding of the sulfate group and the support when Al^{3+} cation was modified into the SiO_2–TiO_2 structure, whereas half of the sulfate concentration was detected on the surface of the final powder (S/SiTi) compared with its parent solution. It can be concluded that the sulfate groups were not purchased on the surface of SiTi as support or agglomerated on the surface, which was not detected in this region of the catalyst surface [49, 58].

Catalyst performance
Catalytic activity in the esterification reaction

According to the literature [59, 60], the esterification reaction over various catalysts
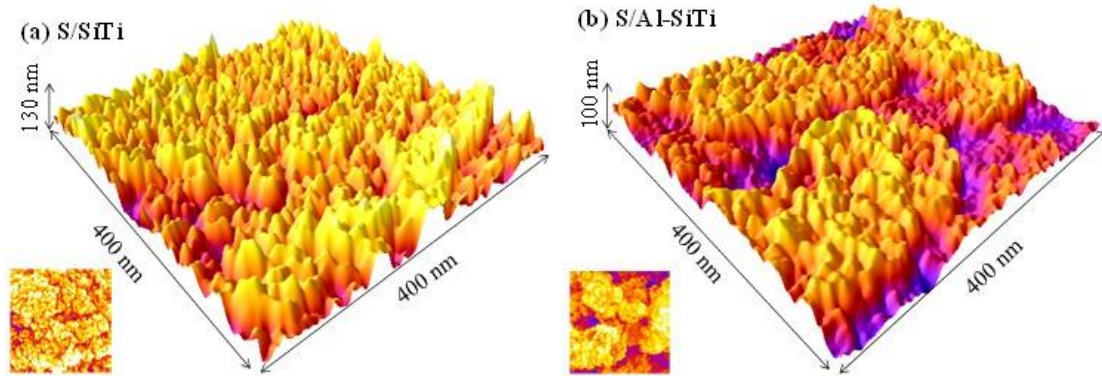
Fig. 5. 3D surface overview of (a) sulfated silica-titania catalyst and (b) sulfated silica-titania catalyst modified by aluminum cation

is carried out at around 120°C, and all the synthesized catalysts exhibited good activities under a methanol/oleic acid molar ratio of 9:1, 3 wt.% catalyst, and the reaction run time of 4 h. The results of the catalytic activity of the samples in the esterification reaction are illustrated in Fig. 7. The synthesized samples exhibited high activity (over 94%, except for the S/SiTi catalyst modified

by Zr^{4+} and Zn^{2+}) in the esterification reaction at 120°C. This can probably be due to their smaller surface area, mean pore size, and acidity. Since the reaction temperature has a direct relationship with the reaction rate, the reaction temperature was decreased to 90°C for better assessment of the activity of the catalysts. Among the samples, the S/Al-SiTi catalyst exhibited less reduction in
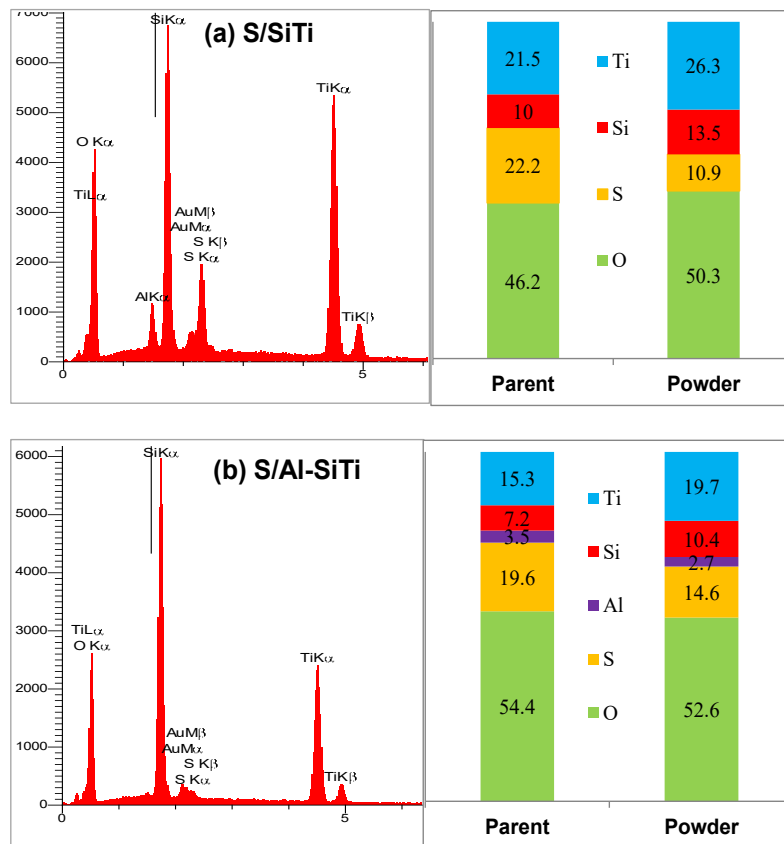
Fig. 6. EDS images of (a) sulfated silica-titania catalyst and (a) sulfated silica-titania catalyst modified by aluminum cation
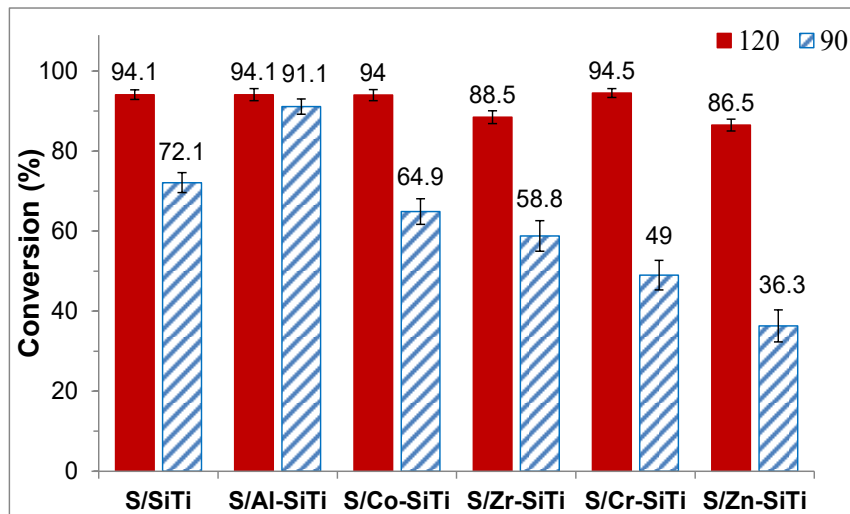
Fig. 7. Activity of sulfated silica-titania catalyst; and sulfated silica-titania modified by aluminum, cobalt, zirconium, chromium and zinc cations (reaction conditions: 9 molar ratio of methanol/oleic acid, 3 wt.% of catalyst and 4 h of reaction time)

the conversion of oleic acid. It seems likely that increasing the interaction between the metal cations and sulfate groups, surface area, mean pore size and reducing the particle size of the support led the S/Al-SiTi catalyst to exhibit the highest activity in the esterification reaction. Komintarachat et al. [61] reported that a solid acid catalyst containing Al_2O_3 as a porous support had higher surface area and greater pore volume compared with those including SiO_2 and ZnO. Large pores can facilitate the easy diffusion of fatty acid molecules in the internal surface area and active sites, resulting in the highest activities in the esterification reaction. Rahmani Vahid et al. [55] also showed that alumina-supported sulfated zirconia had the best catalytic activity in the esterification reaction due to its low crystalline size, well-bonded sulfate groups with zirconium and aluminum ions, and high acidity. They also reported that adding alumina enhanced the reusability of the nanocatalysts. Yee et al. [62] prepared a sulfated zirconia catalyst loaded on alumina for the transesterification of Jatropha Curcas L. oil with methanol to biodiesel and the catalyst had the basic characteristic of an acidic catalyst.

In this study, the nanocatalysts modified with Al^{3+} cations exhibited the highest acidity (1.98 mmol/g). Although S/Al-SiTi (184 m^2/g) had the highest surface area after S/Cr-SiTi (206 m^2/g) nanocatalysts, S/Al-SiTi nanocatalysts exhibited higher pore volume (0.63 cc/g) and mean pore size

(8.9 nm). The proper textural properties of S/Al-SiTi nanocatalysts helped the reactant molecules to be able to truly make a connection with all the available surface area and active sites (especially in porosities), which resulted in higher activity in the esterification reaction [63].

Optimization of the esterification reaction conditions

After selecting S/Al-SiTi nanocatalyst as the most active catalyst, several reaction parameters, including the molar ratio of methanol to oleic acid, reaction time, reaction temperature, and amount of catalyst to oleic acid were examined to obtain an appropriate conversion in the optimum reaction conditions and the obtained results are present in Table 2.

The reaction temperature is an important factor that leads to accelerating the reaction rate as shown in Fig. 7. The results revealed that the conversion using the S/Al-SiTi catalyst drastically reduced to 73.8% by reducing the reaction temperature to 65°C. Therefore, the temperature of 90°C was selected as the optimum temperature.

Maximum conversion of oleic acid into methyl oleate can be ensured by using the excess methanol due to the fact that esterification is a reversible reaction [55]. Increasing the molar ratio of methanol/oleic acid from 3:1 to 9:1 considerably enhanced the conversion from 23.2% to 91.1%. However, further increase in the amount of methanol leads to the reduction of the

Table 2. Optimization of esterification reaction conditions

Run	Temperature (°C)	Methanol/Oleic acid molar ratio	Catalyst amount (wt.% to oleic acid)	time (h)	Conversion (%)
1	65	9:1	3	4	73.8±3.1
2	90	9:1	3	4	91.1±1.9
3	120	9:1	3	4	94.1±1.5
4	90	3:1	3	4	23.2±5.1
5	90	6:1	3	4	80.6±2.2
6	90	12:1	3	4	92.5±1.2
7	90	15:1	3	4	86.7±1.5
8	90	9:1	2	4	82±1.4
9	90	9:1	4	4	91.1±1.7
10	90	9:1	3	2	73.5±2.9
11	90	9:1	3	3	90.7±2
12	90	9:1	3	5	93.0±1.8

conversion. This is probably due to the dilution of the reaction medium, filling the catalyst pores, and covering the active acid sites on the surface. Additionally, this offers better miscibility of methyl oleate and water which could raise the cost of production [10].

The amount of catalyst is also an essential factor in the esterification reaction to provide the required surfaces for the interaction of the reactants and active sites. Therefore, the effect of the catalyst was also studied between 2-4 wt.%. It was found that 3 wt.% catalyst provided sufficient catalyst surfaces to push the esterification reaction towards the maximum conversion, and a higher catalyst loading had an insignificant effect [54]. It is well established that the esterification reaction is a reversible reaction. At low catalyst amounts, there were not enough active sites for the reaction while the reverse reaction might take place when an excessive amount of catalyst was employed [61].

The reaction time was also examined and varied from 2 to 5 h while the other process conditions were kept constant at 90°C, 9:1 molar ratio of methanol/oleic acid, and 3 wt.% catalyst. By raising the reaction time from 2 h to 3 h, a slight increase in the conversion was observed.

Reusability assessment

The reusability of S/Al-SiTi catalyst was also assessed in order to evaluate the catalyst stability and to understand the effect of the loading of Al^{3+} cation on the stability of the sulfated silica-titania catalyst. After each run, the catalyst particles were separated and washed several times with a mixture of methanol/n-hexane (1:1 vol.%) to remove any remaining methyl oleate and oleic acid from the surface and pores of the recovered catalyst. The collected particles were finally oven-dried overnight and then calcined at 300°C for 2 h. The reusability of the catalyst was plotted based on the activity reduction measured using Equation 3.

$$Activity\ reduction\ (\%) = \frac{Conversion\ in\ 1^{st}\ run - conversion\ in\ n^{th}\ run}{Conversion\ in\ first\ run} \quad (3)$$

As observed in Fig. 8, the S/SiTi catalyst drastically lost its catalytic activity after the first run. This might be due to the leaching of the
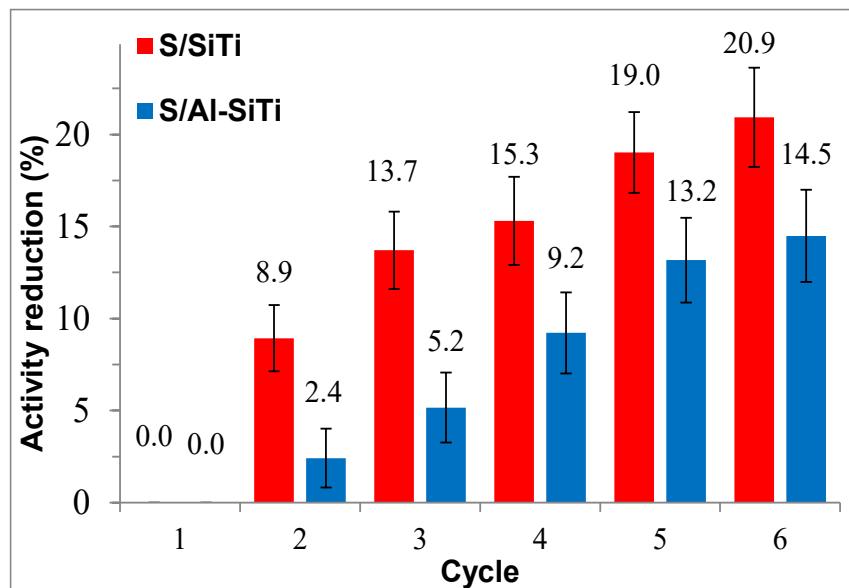
Fig. 8. Reusability of sulfated silica-titania catalyst and sulfated silica-titania catalyst modified by aluminum cation

sulfate groups from the surface of the catalyst in the reaction medium. This result was also consistent with that of the studies on the sulfated silica-titania catalyst [28]. In the case of catalyst modified by Al^{3+} cation, the sulfate groups make stronger bonds with the catalyst surface, and the catalyst shows better stability in the esterification reaction with a conversion greater than 85% through five consecutive runs.

Comparison of the results

The catalytic activity and stability of $SO_4/SiO_2–TiO_2$ modified by the aluminum cation compared with those of some solid acid catalysts reported in the literature are summarized in Table 3. The catalyst synthesized in the current study converted an appropriate amount of oleic acid feedstock into methyl oleate at a lower reaction temperature and shorter time. Moreover, the sample exhibited higher stability for several uses. These desirable properties can be due to the presence of the Al^{3+} cation, which may consequently increase the metal cation-SO_4 bands as well as the acidity [37]. Therefore, the leaching of the sulfate group may reduce.

CONCLUSIONS

Sulfated silica and titania as catalysts were widely studied in many catalytic reactions including esterification and transesterification reactions. However, these solid acid catalysts suffer from a low number of acid sites and weak bonding of sulfate groups with the catalyst surface. Therefore, the metal cations of Al, Co, Zr, Cr, and Zn were reinforced on the sulfated silica-titania catalyst to form a ternary metal oxide system to overcome these problems. The sol-gel method was utilized for the fabrication of the catalysts, and different techniques were used to analyze the physical-chemical properties of the catalysts. It was found that the incorporation of metal cations in the sulfated silica-titania catalyst inhibited the formation of $Ti_2(SO_4)_3$ phase. The FTIR analysis confirmed that among the metal cations the catalyst modified by the Al^{3+} cation had an appropriate interaction between the sulfate groups and the metal cation and catalyst support. Therefore, the catalyst showed higher acidity which is an important parameter for the catalytic esterification reaction. The results showed that the S/Al-SiTi catalyst exhibited high catalytic activity in the esterification reaction at a low temperature (90°C). The reaction conditions using this catalyst (S/Al-SiTi) were also optimized, and the reusability of S/SiTi and S/Al-SiTi catalysts was examined under optimized conditions. High stability of S/Al-SiTi along with the high reduction in the activity of S/SiTi after the first reaction could confirm the positive effect of Al^{3+} cation on improving the catalytic activity and stability. The S/Al-SiTi catalyst

Table 3. Comparison of the activity and stability of the synthesized catalysts containing silica and/or titania catalyst verses

	Current study	[28][a]	[33][b]	[31][c]	[64][d]
Feedstock	Oleic acid	Oleic acid	Palmitic acid	Itaconic acid	Octanoic acid
Catalyst	S/Al-SiTi	S/SiTi[a]	S/ZrTi[b]	S/La-SiTi[c]	S/AlSi[d]
Surface area (m²/g)	184	381	54.6	NR	38.5
Pore size (nm)/volume (cc/g)	4.9/0.63	3.1/0.27	Not Reported	Not Reported	Not Reported
Temperature (°C)	90	120	100	120	160
Methanol/FFA ratio	9:1	20:1	20:1	10:1	4.5:1
Catalyst loading (wt.%)	3	10	1.5	4	5
Reaction time (h)	3	3	5	6	3
Conversion (%)	90.7	93.8	95.3	94.3	99.1
Reusability	6 (85%)	1 (20.9%)	5	4 (89%)	7 (85%)

[a] $SO_4/SiO_2–TiO_2$. [b] $ZrO_2–TiO_2@SO_4^{2-}$. [c] $La^{3+}\sim SO_4^{2-}/TiO_2–SiO_2$. [d] $SO_4^{2-}/Al_2O_3–SiO_2$.

can be a good candidate for biodiesel industrial application after conducting further kinetic studies on different chain lengths of the fatty acid composition and/or cheap feedstocks, e.g. waste cooking oil, microalgae oil, and Jatropha oil.

CONFLICT OF INTEREST
The authors declare that there are no conflicts of interest regarding the publication of this manuscript.

REFERENCES
1. Manaf ISA, Embong NH, Khazaai SNM, Rahim MHA, Yusoff MM, Lee KT, et al. A review for key challenges of the development of biodiesel industry. Energy Conversion and Management. 2019;185:508-17.
2. Adu-Mensah D, Mei D, Zuo L, Zhang Q, Wang J. A review on partial hydrogenation of biodiesel and its influence on fuel properties. Fuel. 2019;251:660-8.
3. Kazemifard S, Nayebzadeh H, Saghatoleslami N, Safakish E. Assessment the activity of magnetic KOH/Fe3O4@Al2O3 core–shell nanocatalyst in transesterification reaction: effect of Fe/Al ratio on structural and performance. Environmental Science and Pollution Research. 2018;25(32):32811-21.
4. Ambat I, Srivastava V, Sillanpää M. Recent advancement in biodiesel production methodologies using various feedstock: A review. Renewable and Sustainable Energy Reviews. 2018;90:356-69.
5. Cucciolito ME, Lega M, Papa V, Ruffo F. Simple Zn(II) Salts as Efficient Catalysts for the Homogeneous Trans-Esterification of Methyl Esters. Catalysis Letters. 2016;146(6):1113-7.
6. Mardhiah HH, Ong HC, Masjuki HH, Lim S, Lee HV. A review on latest developments and future prospects of heterogeneous catalyst in biodiesel production from non-edible oils. Renewable and Sustainable Energy Reviews. 2017;67:1225-36.
7. Xu X, Jiang E, Lei Z. Esterification of guaiacol with octanoic acid over functionalized mesoporous silica. Renewable Energy. 2018;119:439-46.
8. Carlucci C, Degennaro L, Luisi R. Titanium Dioxide as a Catalyst in Biodiesel Production. Catalysts. 2019;9(1):75.
9. Nayebzadeh H, Haghighi M, Saghatoleslami N, Tabasizadeh M, Yousefi S. Fabrication of carbonated alumina doped by

calcium oxide via microwave combustion method used as nanocatalyst in biodiesel production: Influence of carbon source type. Energy Conversion and Management. 2018;171:566-75.

10. Hojjat M, Nayebzadeh H, Khadangi-Mahrood M, Rahmani-Vahid B. Optimization of process conditions for biodiesel production over CaO–Al2O3/ZrO2 catalyst using response surface methodology. Chemical Papers. 2016;71(3):689-98.

11. Nayebzadeh H, Saghatoleslami N, Tabasizadeh M. Application of microwave irradiation for fabrication of sulfated ZrO2–Al2O3 nanocomposite via combustion method for esterification reaction: process condition evaluation. Journal of Nanostructure in Chemistry. 2019;9(2):141-52.

12. Embong NH, Maniam GP, Ab. Rahim MH, Lee KT, Huisingh D. Utilization of palm fatty acid distillate in methyl esters preparation using SO_4^{2-}/TiO_2–SiO_2 as a solid acid catalyst. Journal of Cleaner Production. 2016;116:244-248.

13. Safaei P, Sepahvand S, Hossieni F, Ghasemi S, Sanaee Z. Improving the performance of Lithium-Sulfur Batteries using Sulfur-(TiO2/SiO2) yolk–shell Nanostructure. Journal of Nanostructures. 2020;10(1):76-82.

14. Mahmoud HR, El-Molla SA, Ibrahim MM. Biodiesel production via stearic acid esterification over mesoporous ZrO2/SiO2 catalysts synthesized by surfactant-assisted sol-gel auto-combustion route. Renewable Energy. 2020;160:42-51.

15. Asikin-Mijan N, Lee HV, Taufiq-Yap YH, Abdulkrem-Alsultan G, Mastuli MS, Ong HC. Optimization study of SiO 2 -Al 2 O 3 supported bifunctional acid–base NiO-CaO for renewable fuel production using response surface methodology. Energy Conversion and Management. 2017;141:325-38.

16. Asikin-Mijan N, Lee HV, Marliza TS, Taufiq-Yap YH. Pyrolytic-deoxygenation of triglycerides model compound and non-edible oil to hydrocarbons over SiO 2 -Al 2 O 3 supported NiO-CaO catalysts. Journal of Analytical and Applied Pyrolysis. 2018;129:221-30.

17. Kulyk K, Palianytsia B, Alexander JD, Azizova L, Borysenko M, Kartel M, et al. Kinetics of Valeric Acid Ketonization and Ketenization in Catalytic Pyrolysis on Nanosized SiO2 , γ-Al2 O3 , CeO2 /SiO2 , Al2 O3 /SiO2 and TiO2 /SiO2. ChemPhysChem. 2017;18(14):1943-55.

18. Justine M, Joy Prabu H, Johnson I, Magimai Antoni Raj D, John Sundaram S, Kaviyarasu K. Synthesis and characterizations studies of ZnO and ZnO-SiO2 nanocomposite for biodiesel applications. Materials Today: Proceedings. 2021;36:440-6.

19. Helmiyati H, Suci RP. Nanocomposite of cellulose-ZnO/SiO2 as catalyst biodiesel methyl ester from virgin coconut oil. PROCEEDINGS OF THE 4TH INTERNATIONAL SYMPOSIUM ON CURRENT PROGRESS IN MATHEMATICS AND SCIENCES (ISCPMS2018): AIP Publishing; 2019.

20. Ude CN, Onukwuli DO, Umeuzuegbu JC, Chukwuka CC. Heterogeneously Catalyzed Methanolysis of Gmelina Seed Oil to Biodiesel. Chemical Engineering & Technology. 2020;44(1):65-76.

21. Vidhya R, Gandhimathi R, Sankareswari M, Malliga P, Jeya J, Neivasagam K. Synthesis and Characterization of Cu Doped TiO2 Thin Films to Protect Agriculturally Beneficial Rhizobium and Phosphobacteria from UV Light. Journal of Nanostructures. 2018;8(3):232-241.

22. Mazhari MP, Abbasi A, Derakhshan A, Ahmadi M. Fabrication Fe3O4/SiO2/TiO2 Nanocomposites and Degradation

of Rhodamine B Dyes under UV Light Irradiation. Journal of Nanostructures. 2016;6(1):101-105.

23. Safakish E, Nayebzadeh H, Saghatoleslami N, Kazemifard S. Comprehensive assessment of the preparation conditions of a separable magnetic nanocatalyst for biodiesel production from algae. Algal Research. 2020;49:101949.

24. Nayebzadeh H, Naderi F, Rahmanivahid B. Assessment the synthesis conditions of separable magnetic spinel nanocatalyst for green fuel production: Optimization of transesterification reaction conditions using response surface methodology. Fuel. 2020;271:117595.

25. Gardy J, Nourafkan E, Osatiashtiani A, Lee AF, Wilson K, Hassanpour A, et al. A core-shell SO4/Mg-Al-Fe3O4 catalyst for biodiesel production. Applied Catalysis B: Environmental. 2019;259:118093.

26. Gardy J, Rehan M, Hassanpour A, Lai X, Nizami A-S. Advances in nano-catalysts based biodiesel production from non-food feedstocks. Journal of Environmental Management. 2019;249:109316.

27. Manga J, Ahmad A, Taba P, Firdaus. Potential of palm fatty acid distillate as a feedstock in the synthesis of ethyl esters using solid SO4 2-/TiO2-SiO2 catalysts. IOP Conference Series: Earth and Environmental Science. 2020;473(1):012095.

28. Shao GN, Sheikh R, Hilonga A, Lee JE, Park Y-H, Kim HT. Biodiesel production by sulfated mesoporous titania–silica catalysts synthesized by the sol–gel process from less expensive precursors. Chemical Engineering Journal. 2013;215-216:600-7.

29. Sheikh R, Shao GN, Khan Z, Abbas N, Kim H-T, Park Y-H. Esterification of oleic acid by heteropolyacid/TiO2□SiO2catalysts synthesized from less expensive precursors. Asia-Pacific Journal of Chemical Engineering. 2015;10(3):339-46.

30. Berrones-Hernández R, del Carmen Pérez-Luna Y, Sánchez-Roque Y, Pantoja-Enríquez J, Grajales-Penagos AL, López-Cruz CF, et al. Heterogeneous Esterification of Waste Cooking Oil with Sulfated Titanium Dioxide (STi). BioEnergy Research. 2019;12(3):653-64.

31. Li L, Liu S, Xu J, Yu S, Liu F, Xie C, et al. Esterification of itaconic acid using Ln∼SO42−/TiO2–SiO2 (Ln=La3+, Ce4+, Sm3+) as catalysts. Journal of Molecular Catalysis A: Chemical. 2013;368-369:24-30.

32. Feyzi M, Shahbazi E. Catalytic performance and characterization of Cs–Ca/SiO2–TiO2 nanocatalysts for biodiesel production. Journal of Molecular Catalysis A: Chemical. 2015;404-405:131-8.

33. Fan M, Si Z, Sun W, Zhang P. Sulfonated ZrO2-TiO2 nanorods as efficient solid acid catalysts for heterogeneous esterification of palmitic acid. Fuel. 2019;252:254-61.

34. Kong PS, Pérès Y, Wan Daud WMA, Cognet P, Aroua MK. Esterification of Glycerol With Oleic Acid Over Hydrophobic Zirconia-Silica Acid Catalyst and Commercial Acid Catalyst: Optimization and Influence of Catalyst Acidity. Front Chem. 2019;7:205-.

35. Tai Z, Isaacs MA, Durndell LJ, Parlett CMA, Lee AF, Wilson K. Magnetically-separable Fe3O4@SiO2@SO4-ZrO2 core-shell nanoparticle catalysts for propanoic acid esterification. Molecular Catalysis. 2018;449:137-41.

36. Yuan Y, Jiang W, Li J. Preparation of solid acid catalyst SO42−/TiO2/γ-Al2O3 for esterification: A study on catalytic reaction mechanism and kinetics. Chinese Journal of Chemical Engineering. 2019;27(11):2696-704.

37. Gardy J, Osatiashtiani A, Céspedes O, Hassanpour A, Lai X,

Lee AF, et al. A magnetically separable SO4/Fe-Al-TiO2 solid acid catalyst for biodiesel production from waste cooking oil. Applied Catalysis B: Environmental. 2018;234:268-78.

38. Corro G, Pal U, Tellez N. Biodiesel production from Jatropha curcas crude oil using ZnO/SiO2 photocatalyst for free fatty acids esterification. Applied Catalysis B: Environmental. 2013;129:39-47.

39. Madhuvilakku R, Piraman S. Biodiesel synthesis by TiO2–ZnO mixed oxide nanocatalyst catalyzed palm oil transesterification process. Bioresource Technology. 2013;150:55-9.

40. Sistani A, Saghatoleslami N, Nayebzadeh H. Influence of calcination temperature on the activity of mesoporous CaO/TiO2–ZrO2 catalyst in the esterification reaction. Journal of Nanostructure in Chemistry. 2018;8(3):321-31.

41. Mehdizadeh P, Tavangar Z, Shabani N, Hamadanian M. Visible Light Activity of Nitrogen-Doped TiO2 by Sol-Gel Method Using Various Nitrogen Sources. Journal of Nanostructures. 2020;10(2):307-316.

42. Nayebzadeh H, Saghatoleslami N, Haghighi M, Tabasizadeh M, Binaeian E. Comparative assessment of the ability of a microwave absorber nanocatalyst in the microwave-assisted biodiesel production process. Comptes Rendus Chimie. 2018;21(7):676-83.

43. Riazian M. Dependence of Photocatalytic Activity of TiO2-SiO2 Nanopowders. Journal of Nanostructures. 2014;4(4):433-441.

44. Reddy BM, Reddy GK, Rao KN, Katta L. Influence of alumina and titania on the structure and catalytic properties of sulfated zirconia: Beckmann rearrangement. Journal of Molecular Catalysis A: Chemical. 2009;306(1-2):62-8.

45. Feltrin J, De Noni A, Hotza D, Frade JR. Design guidelines for titania-silica-alumina ceramics with tuned anatase to rutile transformation. Ceramics International. 2019;45(5):5179-88.

46. Gardy J, Hassanpour A, Lai X, Ahmed MH. Synthesis of Ti(SO4)O solid acid nano-catalyst and its application for biodiesel production from used cooking oil. Applied Catalysis A: General. 2016;527:81-95.

47. Ghalandari A, Taghizadeh M, Rahmani M. Statistical Optimization of the Biodiesel Production Process Using a Magnetic Core-Mesoporous Shell KOH/Fe3 O4 @γ -Al2 O3 Nanocatalyst. Chemical Engineering & Technology. 2018;42(1):89-99.

48. Adán C, Carbajo J, Bahamonde A, Oller I, Malato S, Martínez-Arias A. Solar light assisted photodegradation of phenol with hydrogen peroxide over iron-doped titania catalysts: Role of iron leached/readsorbed species. Applied Catalysis B: Environmental. 2011;108-109:168-76.

49. Nayebzadeh H, Haghighi M, Saghatoleslami N, Alaei S, Yousefi S. Texture/phase evolution during plasma treatment of microwave-combustion synthesized KOH/Ca12A-l14O33-C nanocatalyst for reusability enhancement in conversion of canola oil to biodiesel. Renewable Energy. 2019;139:28-39.

50. Shahedi Z, Mansoori Y. Fe₃O₄@SiO₂–SO₃H Nanoparticles: An efficient magnetically retrievable catalyst for esterification reactions. Journal of Particle Science & Technology. 2018;4(2):67-79.

51. Matmin J, Affendi I, Endud S. Direct-Continuous Preparation of Nanostructured Titania-Silica Using Surfactant-Free Non-Scaffold Rice Starch Template. Nanomaterials (Basel). 2018;8(7):514.

52. Chmielarz L, Gil B, Kuśtrowski P, Piwowarska Z, Dudek B, Michalik M. Montmorillonite-based porous clay heterostructures (PCHs) intercalated with silica–titania pillars—synthesis and characterization. Journal of Solid State Chemistry. 2009;182(5):1094-104.

53. Gardy J, Hassanpour A, Lai X, Ahmed MH, Rehan M. Biodiesel production from used cooking oil using a novel surface functionalised TiO2 nano-catalyst. Applied Catalysis B: Environmental. 2017;207:297-310.

54. Teo SH, Islam A, Chan ES, Thomas Choong SY, Alharthi NH, Taufiq-Yap YH, et al. Efficient biodiesel production from Jatropha curcus using CaSO4/Fe2O3-SiO2 core-shell magnetic nanoparticles. Journal of Cleaner Production. 2019;208:816-26.

55. Rahmani Vahid B, Saghatoleslami N, Nayebzadeh H, Toghiani J. Effect of alumina loading on the properties and activity of SO42−/ZrO2 for biodiesel production: Process optimization via response surface methodology. Journal of the Taiwan Institute of Chemical Engineers. 2018;83:115-23.

56. Yousefi S, Haghighi M, Rahmani Vahid B. Role of glycine/nitrates ratio on structural and texture evolution of MgO-based nanocatalyst fabricated by hybrid microwave-impregnation method for biofuel production. Energy Conversion and Management. 2019;182:251-61.

57. Amani T, Haghighi M, Rahmanivahid B. Microwave-assisted combustion design of magnetic Mg–Fe spinel for MgO-based nanocatalyst used in biodiesel production: Influence of heating-approach and fuel ratio. Journal of Industrial and Engineering Chemistry. 2019;80:43-52.

58. Azmoon A-H, Ahmadpour A, Nayebzadeh H, Saghatoleslami N, Heydari A. Fabrication of nanosized SO42−/Co–Al mixed oxide via solution combustion method used in esterification reaction: effect of urea-nitrate ratio on the properties and performance. Journal of Nanostructure in Chemistry. 2019;9(4):247-58.

59. Zhou Y, Niu S, Li J. Activity of the carbon-based heterogeneous acid catalyst derived from bamboo in esterification of oleic acid with ethanol. Energy Conversion and Management. 2016;114:188-96.

60. Gopinath S, Kumar PSM, Arafath KAY, Thiruvengadaravi KV, Sivanesan S, Baskaralingam P. Efficient mesoporous SO42−/Zr-KIT-6 solid acid catalyst for green diesel production from esterification of oleic acid. Fuel. 2017;203:488-500.

61. Komintarachat C, Chuepeng S. Solid Acid Catalyst for Biodiesel Production from Waste Used Cooking Oils. Industrial & Engineering Chemistry Research. 2009;48(20):9350-3.

62. Yee KF, Lee KT, Abdullah AZ, Wu JCS. An Alternative Route for the Preparation of Sulfated Zirconia Loaded on Alumina (SZA) for Biodiesel Production: An Optimization Study. Energy Sources, Part A: Recovery, Utilization, and Environmental Effects. 2013;35(14):1296-305.

63. Jacobson K, Gopinath R, Meher L, Dalai A. Solid acid catalyzed biodiesel production from waste cooking oil. Applied Catalysis B: Environmental. 2008;85(1-2):86-91.